HHS Public Access

Author manuscript

J Invest Dermatol. Author manuscript; available in PMC 2021 May 10.

Published in final edited form as:

J Invest Dermatol. 2018 March ; 138(3): 500–510. doi:10.1016/j.jid.2017.09.024.

Delayed Hair Follicle Morphogenesis and Hair Follicle Dystrophy in a Lipoatrophy Mouse Model of *Pparg* Total Deletion

Chiara Sardella[1,5], **Carine Winkler**[1], **Laure Quignodon**[1], **Jonathan A. Hardman**[2], **Barbara Toffoli**[1], **Greta Maria Paola Giordano Attianese**[1], **Jennifer E. Hundt**[3], **Liliane Michalik**[1], **Charles R. Vinson**[4], **Ralf Paus**[2], **Béatrice Desvergne**[1], **Federica Gilardi**[1]

[1]Center for Integrative Genomics, Faculty of Biology and Medicine, University of Lausanne, Lausanne, Switzerland; [2]Centre for Dermatology Research, School of Biological Sciences, University of Manchester, Manchester, UK; [3]Department of Dermatology, University of Lübeck, Lübeck, Germany; [4]Center for Cancer Research, National Cancer Institute, Laboratory of Metabolism, Bethesda, Maryland, USA [5]Current address: Department of Clinical and Experimental Medicine, Section of Endocrinology, University of Pisa, Pisa, Italy

Abstract

PPARγ regulates multiple aspects of skin physiology, including sebocyte differentiation, keratinocyte proliferation, epithelial stem cell survival, adipocyte biology, and inflammatory skin responses. However, the effects of its global deletion, namely of nonredundant key functions of PPARγ signaling in mammalian skin, are yet unknown because of embryonic lethality. Here, we describe the skin and hair phenotype of a whole-body PPARγ-null mouse (*Pparg*$^{\Delta/\Delta}$), obtained by preserving PPARγ expression in the placenta. *Pparg*$^{\Delta/\Delta}$ mice exhibited total lipoatrophy and complete absence of sebaceous glands. Right after birth, hair follicle (HF) morphogenesis was transiently delayed, along with reduced expression of HF differentiation markers and of transcriptional regulators necessary for HF development. Later, adult *Pparg*$^{\Delta/\Delta}$ mice developed scarring alopecia and severe perifollicular inflammation. Skin analyses in other models of lipodystrophy, AZIP$^{tg/+}$ and *Adipoq-Cre*$^{tg/+}$*Pparg*$^{fl/fl}$ mice, coupled with skin graft experiments, showed that the early defects observed in hair morphogenesis were caused by the absence of adipose tissue. In contrast, the late alteration of HF cycle and appearance of inflammation were observed only in *Pparg*$^{\Delta/\Delta}$ mice and likely were due to the lack sebaceous glands. Our findings underscore the increasing appreciation for the importance of adipose tissue-mediated signals in HF development and function.

Correspondence: Federica Gilardi, Center for Integrative Genomics, University of Lausanne, Genopode Building, CH-1015 Lausanne, Switzerland. Federica.Gilardi@unil.ch.

CONFLICT OF INTEREST

The authors state no conflict of interest.

SUPPLEMENTARY MATERIAL

Supplementary material is linked to the online version of the paper at www.jidonline.org, and at https://doi.org/10.1016/j.jid.2017.09.024.

INTRODUCTION

PPARγ is a nuclear receptor activated by fatty acid metabolites and synthetic compounds such as thiazolidinediones (Desvergne et al., 2004; Straus and Glass, 2007; Varga et al., 2011). PPARγ was first described as the master regulator of adipogenesis and sebocyte differentiation (Barak et al., 1999; Rosen et al., 1999), but it is also involved in metabolic homeostasis maintenance, in the control of immune cell differentiation, and in inflammatory response regulation (reviewed in Ahmadian et al., 2013; Desvergne et al., 2006).

In mammalian skin, besides its prominent expression in adipocytes (Chon and Pappas, 2015; Ramot et al., 2015), PPARγ is highly expressed in suprabasal keratinocytes (Icre et al., 2006), where it inhibits cell proliferation and promotes epidermal differentiation, thus regulating skin barrier permeability (Adachi et al., 2013). PPARγ is also expressed in pilosebaceous units, including, but not restricted to, hair matrix keratinocytes, dermal papilla cells, the inner root sheath (IRS) of the hair follicle (HF) (Billoni et al., 2000), and sebocytes (Dozsa et al., 2014).

Murine hair morphogenesis starts before birth and is accomplished within the first two postnatal weeks, relying on stringently coordinated epithelial-mesenchymal interactions that ultimately result in differentiation of hair shaft, root sheaths, and dermal papilla. Once formed, HFs undergo successive cycles of growth (anagen), regression (catagen), and rest (telogen) (Fuchs and Horsley, 2008; Muller-Rover et al., 2001; Paus et al., 1999; Schmidt-Ullrich and Paus, 2005; Sennett and Rendl, 2012; Sennett et al., 2015). The sebaceous gland (SG) duct is thought to affect the disintegration of the upward-moving IRS where both structures meet (Stenn and Paus, 2001), and SG function/dysfunction may directly influence HF epithelial stem cell compartment and the bulge (Stenn et al., 2008; Sundberg et al., 2000). Therefore, proper SG development and function are critical for HF physiology (Fuchs, 2007; Fuchs and Horsley, 2008).

The importance of PPARγ in HF function emerged with the finding that its targeted deletion in keratin (Krt) 15^{+} murine HF epithelial stem cells leads to accumulation of proinflammatory lipids, resulting in scarring alopecia and SG atrophy in adult mice (Karnik et al., 2009). In human HFs, PPARγ activation enhances the expression of two keratins expressed by HF progenitor cells, Krt15 and Krt19 (Ramot et al., 2014). Moreover, continuous PPARγ signaling was proposed as a protective mechanism to maintain epithelial HF stem cells (Ramot et al., 2015). However, although PPARγ agonists exert beneficial effects in some patients with scarring alopecia (Mesinkovska et al., 2015; Mirmirani and Karnik, 2009), the role of PPARγ signaling in the development of focal lesions of scarring alopecia in patients with lichen-planopilaris or frontal fibrosing alopecia, was questioned (Harries et al., 2013).

Therefore, appropriate mouse models are needed that permit one to comprehensively dissect the role of PPARγ in HF physiology and pathology. Although mice with targeted, tissue-specific PPARγ deletion were developed (reviewed in Ahmadian et al., 2013), constitutive, whole-body PPARγ-knockout is embryonically lethal in mice (Barak et al., 1999). To overcome this limitation, we generated a whole-body PPARγ-null mouse model (*Pparg*$^{\Delta/\Delta}$)

rescued from embryonic lethality by preserving PPARγ expression in the trophoblast (Nadra et al., 2010).

This mouse model permits one to study the consequences of the constitutive absence of functional PPARγ in the entire organism and to specifically dissect nonredundant key functions of PPARγ signaling in mammalian skin. *Pparg*$^{\Delta/\Delta}$ mice suffer from a generalized lipoatrophy, lack SGs, show delayed HF morphogenesis, and develop scarring alopecia as adults. Moreover, our results show a role for adipose tissue in HF morphogenesis, to our knowledge previously unreported.

RESULTS

Pparg$^{\Delta/\Delta}$ mice exhibit delayed postnatal hair growth, HF dystrophy, and subsequent alopecia at the adult stage

We generated *Sox2-Cre*$^{tg/+}$ *Pparg*$^{\Delta/em\Delta}$ (*Pparg*$^{\Delta/\Delta}$) mice through specific epiblastic gene deletion (see Supplementary Figure S1 online). Consistent with the master role of PPARγ in adipogenesis, *Pparg*$^{\Delta/\Delta}$ mice were completely lipoatrophic. At 2–3 days after birth, mutant mice exhibited delayed hair appearance (Figure 1a). At postnatal day (P) 8, the coats of mutant mice had a rough appearance, with short hair over the entire body (see Supplementary Figure S2a online). Thereafter, the skin appeared dry, with moderate white flaking, particularly highlighted after shaving (see Supplementary Figure S2b). At P28 and P49, mutant fur remained altered, with shorter hair than control littermates (Figure 1a, and see Supplementary Figure S2a). With aging, all mutant mice displayed progressive hair loss, which occurred randomly (Figure 1a, and see Supplementary Figure S2c). In addition, 1 out of 10 *Pparg*$^{\Delta/\Delta}$ mice exhibited skin lesions (see Supplementary Figure S2d). No other macroscopic abnormalities were observed in tail hair, vibrissae, nails, or teeth.

Histological analyses of young (P28) *Pparg*$^{\Delta/\Delta}$ skin showed hyperkeratosis and hyperplasia of the interfollicular epidermis (Figure 1b). The dermis showed increased cellularity, which suggested the presence of interstitial inflammation, and intradermal adipocytes and SGs were totally missing (Figure 1b, and see Supplementary Figure S3 online). The subcutaneous fat layer was also absent.

A thorough characterization of skin appendages in *Pparg*$^{\Delta/\Delta}$ mice showed general structural defects in HFs (details in Figure 1c), which resembled HFs damaged by chemotherapy (Hendrix et al., 2005). These defects were accompanied, at P28, by clusters of active phagocytic cells (major histocompatibility complex class II^{+}) around the HFs. Anti-CD45 staining of hematopoietic cells confirmed the presence, in *Pparg*$^{\Delta/\Delta}$ skin, of inflammatory infiltrates, mainly composed of macrophages (F4/80^{+}) and neutrophils (Ly-6B.2^{+}) (Figure 1d and e). In contrast, no changes were observed in the expression of CD3 (*Cd3e*) (see Supplementary Figure S4 online), which suggested that inflammatory infiltration was not sustained by T lymphocytes. These observations are reminiscent of human scarring alopecia, caused by a destructive inflammatory process that leads to cicatricial HFs as a consequence of irreversible HF stem cell damage (Harries et al., 2013; Harries and Paus, 2010), although the disease end stages, characterized by the complete absence of HF, were not fully recapitulated.

We thus explored hair morphogenesis and the subsequent hair cycling, with quantitative histomorphometry (Paus et al., 1999). At P1, hair morphogenesis score was significantly lower in *Pparg*$^{\Delta/\Delta}$ mice compared with control littermates (Figure 2a), which confirmed the significant delay in postnatal HF development. This difference became minor at P8. We next investigated hair cycling phases (Muller-Rover et al., 2001) and found that entry into catagen/first HF cycle was delayed in *Pparg*$^{\Delta/\Delta}$ skin at P17, with a lower percentage of HFs in catagen compared with control mice (Figure 2b). Conversely, at P28, HF number in late catagen was higher in *Pparg*$^{\Delta/\Delta}$ than control skin. At P49, in control mice, nearly 80% of HFs were in telogen, but in *Pparg*$^{\Delta/\Delta}$ mice, most HFs remained in anagen or catagen.

Altogether, these observations indicated that the absence of PPARγ and/or adipose tissue-mediated signaling was responsible for two distinct effects. The early effects, occurring right after birth, affect HF development with transient delay in HF morphogenesis; the late effects are observed from P17 onward, with the slow down of the hair cycle and HF dystrophy.

HF terminal differentiation and homeostasis are defective in *Pparg*$^{\Delta/\Delta}$ mice

We next evaluated changes in the expression of markers of different HF-cell populations during hair morphogenesis (P1-P5-P8). Overall, mRNA levels of *K6irs* (IRS marker), *Tchh* (expressed in IRS and hair shaft medulla), and hair keratins *mHa2* and *mHa3* (hair shaft cortex markers) were lower in *Pparg*$^{\Delta/\Delta}$ skin than in that of aged-matched controls, particularly at P5. These findings, further sustained by the trichohyalin protein expression pattern (see Supplementary Figure S5a online), confirmed a delay in the initial formation of *Pparg*$^{\Delta/\Delta}$ follicles (Figure 3a). Accordingly, at P5 we observed a significant down-regulation of the transcription factors *Foxn1* and *Msx2*, both involved in regulating IRS and hair differentiation. Conversely, during hair morphogenesis, mutant and control mice showed similar mRNA levels of *Alpl* (dermal papilla marker), *Krt5* (outer root sheath marker), and *Krt15* and *Cd200* (HF stem cells markers) (Figure 3b–d) and no inflammation, as assessed at P1 and P8 (see Supplementary Figure S6 online).

We also measured the expression of the same genes during hair cycling (P17-P28-P49). The expression pattern of *Alpl* and *Krt5* remained unaltered in *Pparg*$^{\Delta/\Delta}$ samples (Figure 3c). However, the asynchrony in hair cycles between control and *Pparg*$^{\Delta/\Delta}$ mice was particularly well illustrated by the mirror-image expression profiles of *K6irs*, *Tchh*, *mHa2,* and *Msx2* at the three time points. Indeed, at P17, P28, and P49, control mRNA levels were low, high, and then low, respectively; conversely, *Pparg*$^{\Delta/\Delta}$ mRNA levels were high, low, and then high, respectively (Figure 3a and b). Trichohyalin protein showed a similar pattern of expression (see Supplementary Figure S5b). *Cd200* and *Krt15* mRNA levels were overall reduced during the different hair cycle stages of mutant mice, which suggested a progressive dysfunction occurring in HF stem cell compartment (Figure 3d), concomitant with the appearance (from P17 onward) of skin inflammation (see Supplementary Figure S6).

These results showed that the early delayed hair morphogenesis in *Pparg*$^{\Delta/\Delta}$ mice was mainly characterized by impaired IRS and HF terminal differentiation, whereas the late phenotype was a combination of inflammation and HF stem cell dysfunction, as assessed in the subsequent hair cycle.

Lipodystrophy is associated with early defective HF postnatal differentiation

The consequences of both the total lack of PPARgamma and the lipoatrophy might contribute to determining the early HF phenotype observed in *Pparg*$^{\Delta/\Delta}$ mice. To clarify their respective contribution, we generated fat-specific *Pparg*-knockout mice (*Adipoq-Cre*$^{tg/+}$ *Pparg*$^{fl/fl}$, referred to as *Pparg*F$^{\Delta/\Delta}$), as previously described (Wang et al., 2013). No mature adipocytes were detectable in *Pparg*F$^{\Delta/\Delta}$ skin, whereas SGs were present and adipocyte precursor markers were expressed at normal levels (see Supplementary Figure S7a and b online). As in *Pparg*$^{\Delta/\Delta}$ mice, the expression of *Tchh, mHa3, Foxn1,* and *Msx2* at P5 was significantly reduced in *Pparg*F$^{\Delta/\Delta}$ mice, and trichohyalin staining further reinforced the hypothesis that the lack of mature adipocytes delays HF morphogenesis (see Supplementary Figure S7c and d).

To exclude that this phenotype is specific to PPARγ-dependent lipodystrophy, we finally explored skin and HF phenotype in AZIP$^{tg/+}$ mice, in which the *Fabp4* promoter drives the expression of a C/EBP dominant negative protein (Moitra et al., 1998). These mice, which have no alteration in *Pparg* alleles, are characterized by a nearly complete ablation of mature adipocytes. In agreement with previous reports (Festa et al., 2011), we detected AZIP transgene expression in the dermis but not in the epidermis of AZIP$^{tg/+}$ mice, which excluded a contribution of keratinocyte defects to their skin phenotype (see Supplementary Figure S8a online). As in *Pparg*$^{\Delta/\Delta}$ mice, mature subcutaneous adipose tissue was undetectable in AZIP$^{tg/+}$ mice (Figure 4d), and adipocyte precursor markers were unaltered (see Supplementary Figure S8b). In contrast to *Pparg*$^{\Delta/\Delta}$, but similar to *Pparg*F$^{\Delta/\Delta}$, AZIP$^{tg/+}$ mice showed normal SGs (Figure 4d). Furthermore, AZIP$^{tg/+}$ hair was not evident at P5 and looked sparse hair at P17 (see Supplementary Figure S9a online). Quantitative histomorphometry showed that AZIP$^{tg/+}$ HF morphogenesis was delayed (Figure 4a and b), as confirmed by the reduced expression of *K6irs*, *Tchh*, *mHa2*, *mHa3,* and *Foxn1* at P5 (Figure 4c). In contrast, adult AZIP$^{tg/+}$ mice were indistinguishable from their littermate controls (see Supplementary Figure S9a), and no CD45^{+} inflammatory cell or macrophage infiltration were observed in AZIP$^{tg/+}$ skin (Figure 4d and e, and see Supplementary Figure S9b). Altogether, these results indicate that mature adipocytes contributed to coordinate HF differentiation during hair morphogenesis but that they were not required to maintain the late HF homeostasis.

To characterize at the molecular levels the differences lying at the very initial stage of the interaction between adipocytes and the forming of HFs, knowing that mature adipocytes were detectable in control embryonic skin only from embryonic day (E) 17.5 onward (see Supplementary Figure S10 online), we examined global gene expression in skin from *Pparg*$^{\Delta/\Delta}$ and control embryos at E17.5. We found only 31 differentially expressed genes, and among these, 9 were still reduced at P1 and inhibited also in AZIP$^{tg/+}$ skin (Table 1). As expected, several markers of mature adipocytes, including *Fabp4*, *Adipoq*, *Plin1,* and *Rbp4,* were down-regulated in *Pparg*$^{\Delta/\Delta}$ skin. Moreover, *Tshr* and *Bmper,* two genes potentially relevant for HF morphogenesis (Heinke et al., 2013; Moser et al., 2003), were significantly down-regulated.

Skin graft experiments rescue the early delay in HF morphogenesis but not the late skin phenotype observed in *Pparg*$^{\Delta/\Delta}$ mice

To fully confirm the relevance of adipose tissue and its related systemic environment for a timely HF morphogenesis, we engrafted skin biopsy samples from *Pparg*$^{\Delta/\Delta}$ and control embryos onto immunocompromised *Foxn1*$^{nu/nu}$ mice. Until 21 days after engraftment, hair growth and density were similar in control and *Pparg*$^{\Delta/\Delta}$ grafts (Figure 5a). Quantitative histomorphometry analysis performed 7 days after the engraftment showed a complete rescue of *Pparg*$^{\Delta/\Delta}$ delayed HF morphogenesis (Figure 5b and c), consistent with the recovery in the expression of *K6irs*, *Tchh*, *mHa2*, *mHa3*, *Foxn1,* and *Msx2*, whereas *Krt15* remained unaffected (Figure 5d). *Pparg* and *Adipoq* expression in the skin was still significantly reduced, thus arguing against the possible presence of local mature adipocytes within the graft. Similar results were obtained in skin grafts from AZIP$^{tg/+}$ embryos (see Supplementary Figure S11 online). Collectively, these observations show that the altered environment induced by the lack of adipose tissue is responsible for the early effects on HF morphogenesis observed in *Pparg*$^{\Delta/\Delta}$ and AZIP$^{tg/+}$ mice.

In contrast, at later time points, hair loss and inflammation appeared specifically in *Pparg*$^{\Delta/\Delta}$ grafts (Figure 5a), as shown by the increased inflammatory cell infiltration detected in *Pparg*$^{\Delta/\Delta}$ grafts after 38 days (Figure 5e and f), whereas no signs of inflammation were present in AZIP$^{tg/+}$ grafts (see Supplementary Figure S12a and b online). These results, consistent with the late appearance of inflammation only in *Pparg*$^{\Delta/\Delta}$ skin (see Supplementary Figure S6), suggested a direct responsibility for the lack of local PPARγ and the associated absence of SGs on the late HF phenotype of *Pparg*$^{\Delta/\Delta}$ mice, characterized by strong inflammatory response, HF cycle defects, and alopecia.

DISCUSSION

Our results highlight a dramatic skin phenotype in *Pparg*$^{\Delta/\Delta}$ mice, characterized by two main defects at the level of HFs. Right after birth, the complete absence of adipose tissue induces a transient delay of the postnatal HF morphogenesis. The late effects are seen after hair growth, when the lack of PPARγ in HF stem cells, together with the lack of SGs, slows the hair cycle, severely alters HF morphology, and induces skin inflammation.

The late *Pparg*$^{\Delta/\Delta}$ skin phenotype reinforces previous reports that described PPARγ contribution to pilosebaceous unit homeostasis (Fu et al., 2010; Karnik et al., 2009; Nakahigashi et al., 2012; Zhang et al., 2006). In particular, PPARγ absence in bulge HF stem cells and the lack of SGs explain, at least in part, the aberrant hair cycle and chronic inflammation observed in *Pparg*$^{\Delta/\Delta}$ mice starting at P17 and reproduced in our graft experiments. However, additional contributions linked to PPARγ dysfunctions in other cellular compartments cannot be excluded, in that they can induce environmental alterations with a potential impact on HF homeostasis. For instance, the milk produced by females lacking *Pparg* in mammary glands is enriched in toxic lipids that provoke a strong alopecia in the breast-fed pups, starting from P16 (Wan et al., 2007), which shows how sensitive HFs might be to environmental cues. Furthermore, the role of adipose tissue, totally missing in *Pparg*$^{\Delta/\Delta}$ mice, must be considered. Adipocytes are abundantly present in dermis (Driskell et al., 2014; Kruglikov and Scherer, 2016) and have been implicated in wound healing

(Schmidt and Horsley, 2013), homeostatic temperature regulation (Kasza et al., 2014), cutaneous fibrosis (Marangoni et al., 2015), and protection against skin infections (Zhang et al., 2015). The first indications of an adipocyte-HF axis came from mice with reduced intradermal adipose tissue, such as *Fatp4*− and *Dgat1*− and −*2*–deficient mice, exhibiting skin abnormalities and hair loss (Chen et al., 2002; Herrmann et al., 2003; Stone et al., 2004).

However, those observations remained elusive because of additional sebocyte defects, which may have contributed to the observed phenotype. More recently, independent reports have shown that intradermal preadipocytes and differentiated adipocytes secrete factors (Geyfman et al., 2015), such as PDGFA (Festa et al., 2011) and BMP2 (Plikus and Chuong, 2014; Plikus et al., 2008), respectively, that regulate the progression through HF cycling. Recent evidence highlighted that the adipose tissue-HF axis also works in the opposite direction. The appearance of dermal adipocytes in midanagen occurs right after the formation of HF transit-amplifying cells, generated by HF stem cells and secreting the SHH factor, which promotes adipocyte precursor proliferation (Zhang et al., 2016). Thus, the reciprocal communication between HFs and dermal adipocytes ensures the proper progression through HF cycling. Moreover, in other pathophysiological conditions, such as wound healing, HF regeneration occurring in large skin wounds is required for the beneficial conversion of myofibroblasts to adipocytes through the activation of BMP signaling (Plikus et al., 2017).

During skin morphogenesis, although HF formation is not required for the induction and expansion of dermal adipocytes (Donati et al., 2014), our data clearly suggest that mature adipocytes are required for the early initial regulation of hair morphogenesis timing. First, hair growth is delayed in three mouse models with defects in adipocyte maturation, rather than in adipocyte precursors: *Pparg*$^{\Delta/\Delta}$, AZIP$^{tg/+}$, and *Pparg*F$^{\Delta/\Delta}$. Second, no defects are observed when *Pparg*$^{\Delta/\Delta}$ or AZIP$^{tg/+}$ skin is engrafted in the recipient *Foxn1*$^{nu/nu}$ mice, which bear functional adipose tissue. Finally, HF stem cell markers are not altered during HF morphogenesis, which excludes a common mechanism for defective hair morphogenesis and the later occurrence of scarring alopecia.

The appearance of the first lipid-filled adipocytes below the dermis at E17.5 is consistent with previous observations (Birsoy et al., 2011; Driskell et al., 2013) and depends on the activation of the Wnt/β-catenin pathway in the epidermis occurring earlier, at E14.5 (Donati et al., 2014). This timing reinforces the hypothesis that adipose tissue-mediated signals might be implicated during the last stages (i.e., late organogenesis and cytogenesis) of HF morphogenesis, rather than in the initiation phase, which occurs sharply at E14.5 (Schmidt-Ullrich and Paus, 2005). Although our study does not completely clarify the molecular players involved in the crosstalk of adipocytes-HFs at this stage of HF development, we found two interesting candidates of possible adipose-derived paracrine regulators: *Tshr* and *Bmper,* whose expression was defective in *Pparg*$^{\Delta/\Delta}$ skin. Both *Tshr* and *Bmper* are expressed by adipocytes (Bell et al., 2000; Mastrogiannaki et al., 2016) and might potentially influence HF development through the regulation of keratins (Bodo et al., 2008) or by interfering with BMP signaling (Heinke et al., 2013; Moser et al., 2003), respectively. However, we cannot exclude that the lack of dermal adipocytes alters the availability of metabolites required for energy metabolism of surrounding organs (e.g., HFs), similar to

what was observed for fatty acids provided to heart by epicardial fat (Talman et al., 2014). In *Pparg*$^{\Delta/\Delta}$ and AZIP$^{tg/+}$ skin grafts experiments, HF morphogenesis is rescued, even though adipocytes are not always evident in graft sections and *Adipoq* expression remained down-regulated. Thus, at the current state, the involvement of sys-temic cues triggered by the lack of adipose tissue in fine-tuning HF morphogenesis seems plausible.

MATERIALS AND METHODS

In vivo experiments

Animal experiments were approved by the animal experimentation commission of Canton of Vaud, accordingly to the European Community Council Directives (86/609/EEC).

Mouse models

Pparg floxed allele (formerly PPARγL2, hereafter called *Pparg*^{fl}) and *Pparg*-null allele (PPARγL-, hereafter called *Pparg*$^{\Delta}$) were previously described (Imai et al., 2004). Matings to generate *Pparg*$^{\Delta/\Delta}$ using *Sox2-Cre*$^{tg/+}$mice (Jackson Laboratory, Br) are shown in Supplementary Figure S1. AZIP/F1 mice (AZIP$^{tg/+}$) and fat-specific *Pparg*-null mice (*Adipoq-Cre*$^{tg/+}$;*Pparg*$^{fl/fl}$) were generated as previously described (Moitra et al., 1998; Wang et al., 2013).

Skin grafts

Full-thickness skin (1 cm^2) was removed from the torso of E18.5 *Pparg*$^{\Delta/\Delta}$, AZIP$^{tg/+}$, and respective control littermates and grafted onto wounds on the backs of *Foxn1*$^{nu/nu}$ mice, after removal of epidermis and dermis. Grafts were performed in at least eight mice per genotype.

Histology

Full-thickness back skin was either fixed in 4% paraformaldehyde and paraffin embedded or frozen in optimal cutting temperature compound (Sakura, Torrance, CA). 4-μm paraffin sections were stained with hematoxylin and eosin or with anti-F4/80 (ab6640, Abcam, Cambridge, MA), anti-Ly-6B.2 alloantigen (MCA771GA, AbD Serotec, Oxford, UK), anti-trichohyalin (ab58755, Abcam) and anti-Iba1 (019-19741, Wako Chemicals, Richmond, VA), followed by detection with 3,3′-diaminobenzidine or fluorescent secondary antibody. For quantitative histomorphometry, HF morphogenesis was evaluated according to the stages defined in Paus et al. (1999), and hair cycle was evaluated at P17 (catagen), P28 (anagen), and P49 (telogen), according to the Muller-Rover classification (Magerl et al., 2001). Cryosections were stained with Oil Red O (Sigma-Aldrich, St. Louis, MO) or with anti-CD45PE (103105, BioLegend, San Diego, CA), anti-major histocompatibility complex class II (T-2106, BMA Biomedicals, Augst, Switzerland, Switzerland), anti-caveolin1 (3267, Cell Signaling, Danvers, MA), and HCS LipidTOX (H34476, Molecular Probes, Eugene, OR). Staining quantification was performed with Image J software (National Institutes of Health, Bethesda, MD).

Gene expression analyses

Full-thickness skin samples were snap frozen in TRIzol (Invitrogen, Waltham, MA), and RNA was extracted following manufacturer's instructions. For microarrays, 100 ng of total RNA were analyzed on Mouse Gene 1.0ST arrays (Affymetrix, Santa Clara, CA) according to manufacturer's instructions. Statistical analyses were performed with R and various Bioconductor packages (http://www.Bioconductor.org). Normalized expression signals were calculated from Affymetrix CEL files using RMA normalization method. Data are accessible in GEO, series GSE85497. For quantitative real-time–PCR analysis, retrotranscription was performed using iScript cDNA synthesis kit (Bio-Rad Laboratories, Hercules, CA). Real-time PCR was performed using the FastStart Universal SYBR Green Master (Roche Applied Science, Indianapolis, IN) in an ABI Prism 7900 Sequence Detection System (Life Technologies, Carlsbad, CA). Primer sequences are available upon request.

Statistical analyses

Statistical analyses were performed with Student *t* test or two-way analysis of variance (Bonferroni posttest analysis) for comparison of two or multiple groups, respectively, using Prism 5.0 (GraphPad, San Diego, CA). Differences with *P*-values less than 0.05 were considered statistically significant.

Supplementary Material

Refer to Web version on PubMed Central for supplementary material.

ACKNOWLEDGMENTS

We are grateful to the Genome Technologies Facility (University of Lausanne) where microarrays were performed. We thank Catherine Moret and Maude Delacombaz (Center for Integrative Genomics) for their advice and help in histology and Armelle Bauduret and Katharina Hausherr for help in genotyping. This work was financed by the Swiss National Science Foundation and the Etat de Vaud.

Abbreviations:

E	embryonic day
HF	hair follicle
IRS	inner root sheath
Krt	keratin
P	postnatal day
SG	sebaceous gland

REFERENCES

Adachi Y, Hatano Y, Sakai T, Fujiwara S. Expressions of peroxisome proliferator-activated receptors (PPARs) are directly influenced by permeability barrier abrogation and inflammatory cytokines and

depressed PPARalpha modulates expressions of chemokines and epidermal differentiation-related molecules in keratinocytes. Exp Dermatol 2013;22: 606–8. [PubMed: 23947677]

Ahmadian M, Suh JM, Hah N, Liddle C, Atkins AR, Downes M, et al. PPARgamma signaling and metabolism: the good, the bad and the future. Nat Med 2013;19:557–66. [PubMed: 23652116]

Barak Y, Nelson MC, Ong ES, Jones YZ, Ruiz-Lozano P, Chien KR, et al. PPAR gamma is required for placental, cardiac, and adipose tissue development. Mol Cell 1999;4:585–95. [PubMed: 10549290]

Bell A, Gagnon A, Grunder L, Parikh SJ, Smith TJ, Sorisky A. Functional TSH receptor in human abdominal preadipocytes and orbital fibroblasts. Am J Physiol Cell Physiol 2000;279(2):C335–40. [PubMed: 10912999]

Billoni N, Buan B, Gautier B, Collin C, Gaillard O, Mahe YF, et al. Expression of peroxisome proliferator activated receptors (PPARs) in human hair follicles and PPAR alpha involvement in hair growth. Acta Derm Venereol 2000;80:329–34. [PubMed: 11200828]

Birsoy K, Berry R, Wang T, Ceyhan O, Tavazoie S, Friedman JM, et al. Analysis of gene networks in white adipose tissue development reveals a role for ETS2 in adipogenesis. Development 2011;138:4709–19. [PubMed: 21989915]

Bodo E, Kromminga A, Biro T, Borbiro I, Gaspar E, Zmijewski MA, et al. Human female hair follicles are a direct, nonclassical target for thyroid-stimulating hormone. J Invest Dermatol 2008;129:1126–39. [PubMed: 19052559]

Chen HC, Smith SJ, Tow B, Elias PM, Farese RV Jr. Leptin modulates the effects of acyl CoA:diacylglycerol acyltransferase deficiency on murine fur and sebaceous glands. J Clin Invest 2002;109:175–81. [PubMed: 11805129]

Chon SH, Pappas A. Differentiation and characterization of human facial subcutaneous adipocytes. Adipocyte 2015;4:13–21. [PubMed: 26167398]

Desvergne B, Michalik L, Wahli W. Be fit or be sick: peroxisome proliferator-activated receptors are down the road. Mol Endocrinol 2004;18:1321–32. [PubMed: 15087471]

Desvergne B, Michalik L, Wahli W. Transcriptional regulation of metabolism. Physiol Rev 2006;86:465–514. [PubMed: 16601267]

Donati G, Proserpio V, Lichtenberger BM, Natsuga K, Sinclair R, Fujiwara H, et al. Epidermal Wnt/beta-catenin signaling regulates adipocyte differentiation via secretion of adipogenic factors. Proc Natl Acad Sci USA 2014;111:E1501–9. [PubMed: 24706781]

Dozsa A, Dezso B, Toth BI, Bacsi A, Poliska S, Camera E, et al. PPARgamma-mediated and arachidonic acid-dependent signaling is involved in differentiation and lipid production of human sebocytes. J Invest Dermatol 2014;134:910–20. [PubMed: 24129064]

Driskell RR, Jahoda CA, Chuong CM, Watt FM, Horsley V. Defining dermal adipose tissue. Exp Dermatol 2014;23:629–31. [PubMed: 24841073]

Driskell RR, Lichtenberger BM, Hoste E, Kretzschmar K, Simons BD, Charalambous M, et al. Distinct fibroblast lineages determine dermal architecture in skin development and repair. Nature 2013;504(7479): 277–81. [PubMed: 24336287]

Festa E, Fretz J, Berry R, Schmidt B, Rodeheffer M, Horowitz M, et al. Adipocyte lineage cells contribute to the skin stem cell niche to drive hair cycling. Cell 2011;146:761–71. [PubMed: 21884937]

Fu G, Gao Q-G, Lian X-H, Yu J, Xiang M-M, Yang T. Committed differentiation of hair follicle bulge cells into sebocytes: an in vitro study. Int J Dermatol 2010;49:135–40. [PubMed: 20465636]

Fuchs E Scratching the surface of skin development. Nature 2007;445(7130): 834–42. [PubMed: 17314969]

Fuchs E, Horsley V. More than one way to skin. Genes Dev 2008;22:976–85. [PubMed: 18413712]

Geyfman M, Plikus MV, Treffeisen E, Andersen B, Paus R. Resting no more: re-defining telogen, the maintenance stage of the hair growth cycle. Biol Rev Camb Philos Soc 2015;90:1179–96. [PubMed: 25410793]

Harries MJ, Meyer K, Chaudhry I, J EK, Poblet E, Griffiths CE, et al. Lichen planopilaris is characterized by immune privilege collapse of the hair follicle's epithelial stem cell niche. J Pathol 2013;231:236–47. [PubMed: 23788005]

Harries MJ, Paus R. The pathogenesis of primary cicatricial alopecias. Am J Pathol 2010;177:2152–62. [PubMed: 20889564]

Heinke J, Juschkat M, Charlet A, Mnich L, Helbing T, Bode C, et al. Antagonism and synergy between extracellular BMP modulators Tsg and BMPER balance blood vessel formation. J Cell Sci 2013;126:3082–94. [PubMed: 23641068]

Hendrix S, Handjiski B, Peters EM, Paus R. A guide to assessing damage response pathways of the hair follicle: lessons from cyclophosphamide-induced alopecia in mice. J Invest Dermatol 2005;125:42–51. [PubMed: 15982301]

Herrmann T, van der Hoeven F, Grone H-J, Stewart AF, Langbein L, Kaiser I, et al. Mice with targeted disruption of the fatty acid transport protein 4 (Fatp 4, Slc27a4) gene show features of lethal restrictive dermopathy. J Cell Biol 2003;161:1105–15. [PubMed: 12821645]

Icre G, Wahli W, Michalik L. Functions of the peroxisome proliferator-activated receptor (PPAR) alpha and beta in skin homeostasis, epithelial repair, and morphogenesis. J Investig Dermatol Symp Proc 2006;11: 30–5.

Imai T, Takakuwa R, Marchand S, Dentz E, Bornert JM, Messaddeq N, et al. Peroxisome proliferator-activated receptor gamma is required in mature white and brown adipocytes for their survival in the mouse. Proc Natl Acad Sci USA 2004;101:4543–7. [PubMed: 15070754]

Karnik P, Tekeste Z, McCormick TS, Gilliam AC, Price VH, Cooper KD, et al. Hair follicle stem cell-specific PPARgamma deletion causes scarring alopecia. J Invest Dermatol 2009;129:1243–57. [PubMed: 19052558]

Kasza I, Suh Y, Wollny D, Clark RJ, Roopra A, Colman RJ, et al. Syndecan-1 is required to maintain intradermal fat and prevent cold stress. PLoS Genet 2014;10(8):e1004514. [PubMed: 25101993]

Kruglikov IL, Scherer PE. Dermal adipocytes and hair cycling: is spatial heterogeneity a characteristic feature of the dermal adipose tissue depot? Exp Dermatol 2016;25:258–62. [PubMed: 26781768]

Magerl M, Tobin DJ, Muller-Rover S, Hagen E, Lindner G, McKay IA, et al. Patterns of proliferation and apoptosis during murine hair follicle morphogenesis. J Invest Dermatol 2001;116:947–55. [PubMed: 11407986]

Marangoni RG, Korman BD, Wei J, Wood TA, Graham LV, Whitfield ML, et al. Myofibroblasts in murine cutaneous fibrosis originate from adiponectin-positive intradermal progenitors. Arthritis Rheumatol 2015;67:1062–73. [PubMed: 25504959]

Mastrogiannaki M, Lichtenberger BM, Reimer A, Collins CA, Driskell RR, Watt FM. β-catenin stabilization in skin fibroblasts causes fibrotic lesions by reventing adipocyte differentiation of the reticular dermis. J Invest Dermatol 2016;136:1130–42. [PubMed: 26902921]

Mesinkovska NA, Tellez A, Dawes D, Piliang M, Bergfeld W. The use of oral pioglitazone in the treatment of lichen planopilaris. J Am Acad Dermatol 2015;72:355–6. [PubMed: 25592345]

Mirmirani P, Karnik P. Lichen planopilaris treated with a peroxisome proliferator-activated receptor gamma agonist. Arch Dermatol 2009;145: 1363–6. [PubMed: 20026843]

Moitra J, Mason MM, Olive M, Krylov D, Gavrilova O, Marcus-Samuels B, et al. Life without white fat: a transgenic mouse. Genes Dev 1998;12: 3168–81. [PubMed: 9784492]

Moser M, Binder O, Wu Y, Aitsebaomo J, Ren R, Bode C, et al. BMPER, a novel endothelial cell precursor-derived protein, antagonizes bone morphogenetic protein signaling and endothelial cell differentiation. Mol Cell Biol 2003;23:5664–79. [PubMed: 12897139]

Muller-Rover S, Handjiski B, van der Veen C, Eichmuller S, Foitzik K, McKay IA, et al. A comprehensive guide for the accurate classification of murine hair follicles in distinct hair cycle stages. J Invest Dermatol 2001;117:3–15. [PubMed: 11442744]

Nadra K, Quignodon L, Sardella C, Joye E, Mucciolo A, Chrast R, et al. PPARgamma in placental angiogenesis. Endocrinology 2010;151: 4969–81. [PubMed: 20810566]

Nakahigashi K, Doi H, Otsuka A, Hirabayashi T, Murakami M, Urade Y, et al. PGD2 induces eotaxin-3 via PPARgamma from sebocytes: a possible pathogenesis of eosinophilic pustular folliculitis. J Allergy Clin Immunol 2012;129:536–43. [PubMed: 22206772]

Paus R, Muller-Rover S, Van Der Veen C, Maurer M, Eichmuller S, Ling G, et al. A comprehensive guide for the recognition and classification of distinct stages of hair follicle morphogenesis. J Invest Dermatol 1999;113:523–32. [PubMed: 10504436]

Plikus MV, Chuong CM. Macroenvironmental regulation of hair cycling and collective regenerative behavior. Cold Spring Harb Perspect Med 2014;4(1):a015198. [PubMed: 24384813]

Plikus MV, Guerrero-Juarez CF, Ito M, Li YR, Dedhia PH, Zheng Y, et al. Regeneration of fat cells from myofibroblasts during wound healing. Science 2017;355(6326):748–52. [PubMed: 28059714]

Plikus MV, Mayer JA, de la Cruz D, Baker RE, Maini PK, Maxson R, et al. Cyclic dermal BMP signalling regulates stem cell activation during hair regeneration. Nature 2008;451(7176):340–4. [PubMed: 18202659]

Ramot Y, Mastrofrancesco A, Camera E, Desreumaux P, Paus R, Picardo M. The role of PPARgamma-mediated signalling in skin biology and pathology: new targets and opportunities for clinical dermatology. Exp Dermatol 2015;24:245–51. [PubMed: 25644500]

Ramot Y, Mastrofrancesco A, Herczeg-Lisztes E, Biro T, Picardo M, Kloepper JE, et al. Advanced inhibition of undesired human hair growth by PPARgamma modulation? J Invest Dermatol 2014;134:1128–31. [PubMed: 24352039]

Rosen ED, Sarraf P, Troy AE, Bradwin G, Moore K, Milstone DS, et al. PPAR gamma is required for the differentiation of adipose tissue in vivo and in vitro. Mol Cell 1999;4:611–7. [PubMed: 10549292]

Schmidt BA, Horsley V. Intradermal adipocytes mediate fibroblast recruitment during skin wound healing. Development 2013;140:1517–27. [PubMed: 23482487]

Schmidt-Ullrich R, Paus R. Molecular principles of hair follicle induction and morphogenesis. Bioessays 2005;27:247–61. [PubMed: 15714560]

Sennett R, Rendl M. Mesenchymal-epithelial interactions during hair follicle morphogenesis and cycling. Semin Cell Dev Biol 2012;23:917–27. [PubMed: 22960356]

Sennett R, Wang Z, Rezza A, Grisanti L, Roitershtein N, Sicchio C, et al. An integrated transcriptome atlas of embryonic hair follicle progenitors, their niche, and the developing skin. Dev Cell 2015;34:577–91. [PubMed: 26256211]

Stenn KS, Paus R. Controls of hair follicle cycling. Physiol Rev 2001;81: 449–94. [PubMed: 11152763]

Stenn KS, Zheng Y, Parimoo S. Phylogeny of the hair follicle: the sebogenic hypothesis. J Invest Dermatol 2008;128:1576–8. [PubMed: 18079744]

Stone SJ, Myers HM, Watkins SM, Brown BE, Feingold KR, Elias PM, et al. Lipopenia and skin barrier abnormalities in DGAT2-deficient mice. J Biol Chem 2004;279:11767–76. [PubMed: 14668353]

Straus DS, Glass CK. Anti-inflammatory actions of PPAR ligands: new insights on cellular and molecular mechanisms. Trends Immunol 2007;28: 551–8. [PubMed: 17981503]

Sundberg JP, Boggess D, Sundberg BA, Eilertsen K, Parimoo S, Filippi M, et al. Asebia-2J (Scd1(ab2J)): a new allele and a model for scarring alopecia. Am J Pathol 2000;156:2067–75. [PubMed: 10854228]

Talman AH, Psaltis PJ, Cameron JD, Meredith IT, Seneviratne SK, Wong DT. Epicardial adipose tissue: far more than a fat depot. Cardiovasc Diagn Ther 2014;4:416–29. [PubMed: 25610800]

Varga T, Czimmerer Z, Nagy L. PPARs are a unique set of fatty acid regulated transcription factors controlling both lipid metabolism and inflammation. Biochim Biophys Acta 2011;1812:1007–22. [PubMed: 21382489]

Wan Y, Saghatelian A, Chong L-W, Zhang C-L, Cravatt BF, Evans RM. Maternal PPARγ protects nursing neonates by suppressing the production of inflammatory milk. Genes Dev 2007;21:1895–908. [PubMed: 17652179]

Wang F, Mullican SE, DiSpirito JR, Peed LC, Lazar MA. Lipoatrophy and severe metabolic disturbance in mice with fat-specific deletion of PPARgamma. Proc Natl Acad Sci USA 2013;110(46):18656–61. [PubMed: 24167256]

Zhang B, Tsai PC, Gonzalez-Celeiro M, Chung O, Boumard B, Perdigoto CN, et al. Hair follicles' transit-amplifying cells govern concurrent dermal adipocyte production through Sonic Hedgehog. Genes Dev 2016;30: 2325–38. [PubMed: 27807033]

Zhang J, He XC, Tong W-G, Johnson T, Wiedemann LM, Mishina Y, et al. Bone morphogenetic protein signaling inhibits hair follicle anagen induction by restricting epithelial stem/progenitor cell activation and expansion. Stem Cells 2006;24:2826–39. [PubMed: 16960130]

Zhang LJ, Guerrero-Juarez CF, Hata T, Bapat SP, Ramos R, Plikus MV, et al. Innate immunity. Dermal adipocytes protect against invasive Staphylococcus aureus skin infection. Science 2015;347(6217): 67–71. [PubMed: 25554785]

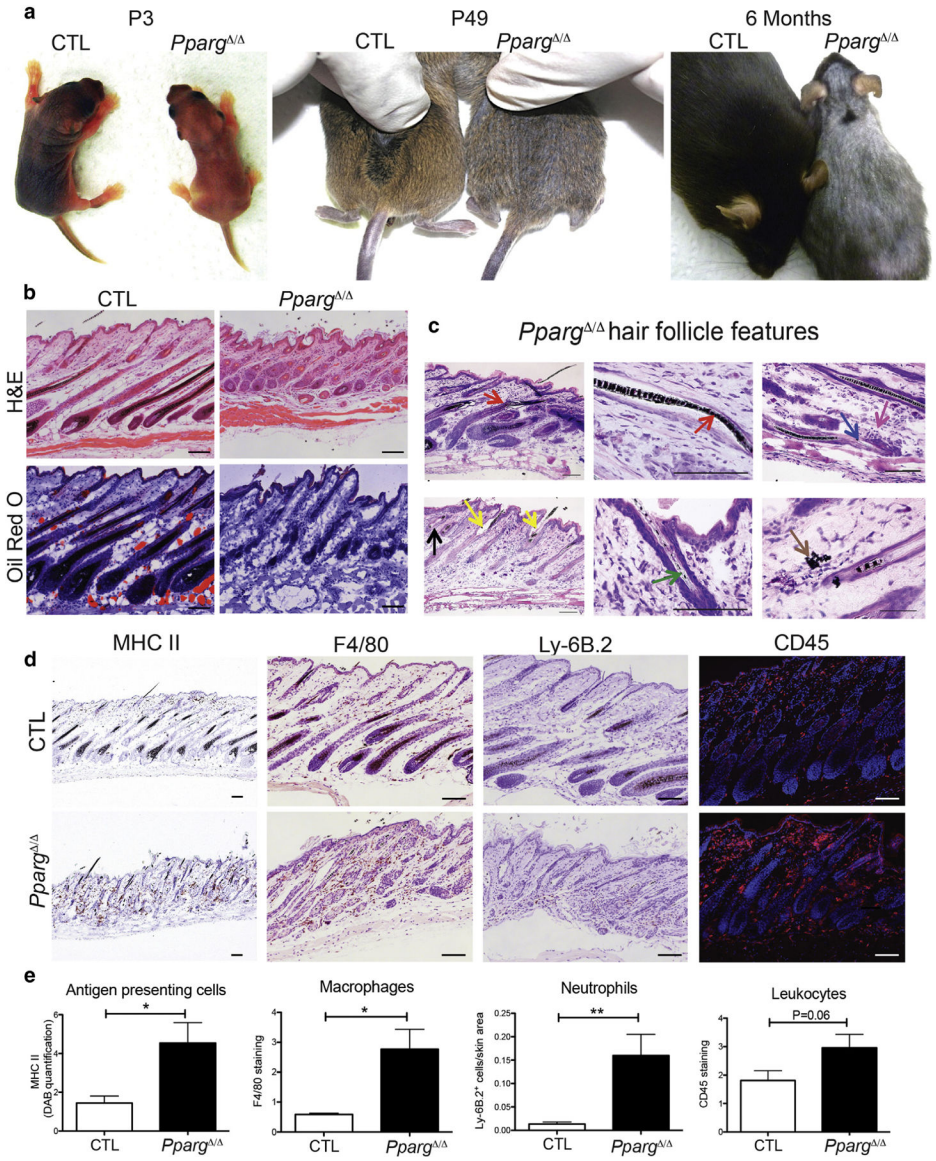

Figure 1. Spontaneous skin and hair phenotype in *Pparg*$^{\Delta/\Delta}$ mice.

(**a**) Pictures of *Sox2-Cre*$^{tg/+}$ *Pparg*$^{\Delta}$/*em*$^{\Delta}$ (*Pparg*$^{\Delta/\Delta}$) and control (CTL) mice at P3, P49, and 6 months. (**b**) Hematoxylin and eosin and Oil Red O staining of back skin sections from *Pparg*$^{\Delta/\Delta}$ and CTL mice at P28. (**c**) Giemsa-staining showing dystrophic features of the HF (arrows) at P28: follicular plugging (black), perifollicular inflammation (fuchsia), HF disruption (blue), or deformation (red) with widened hair canal (yellow), irregular melanin banding pattern (green), and extrafollicular deposits of melanin (brown). (**d**) Immunostaining with anti-MHC II (activated phagocytic cells), anti-F4/80 (macrophages), anti-Ly-6B.2 (neutrophils), and anti-CD45 (leukocytes). (**e**) Quantification of the stainings in **d.** Data expressed as mean ± standard error of the mean (n = 3). Scale bars =100 μm. CTL, control; H&E, hematoxylin and eosin; MHC, major histocompatibility complex; P, postnatal day.

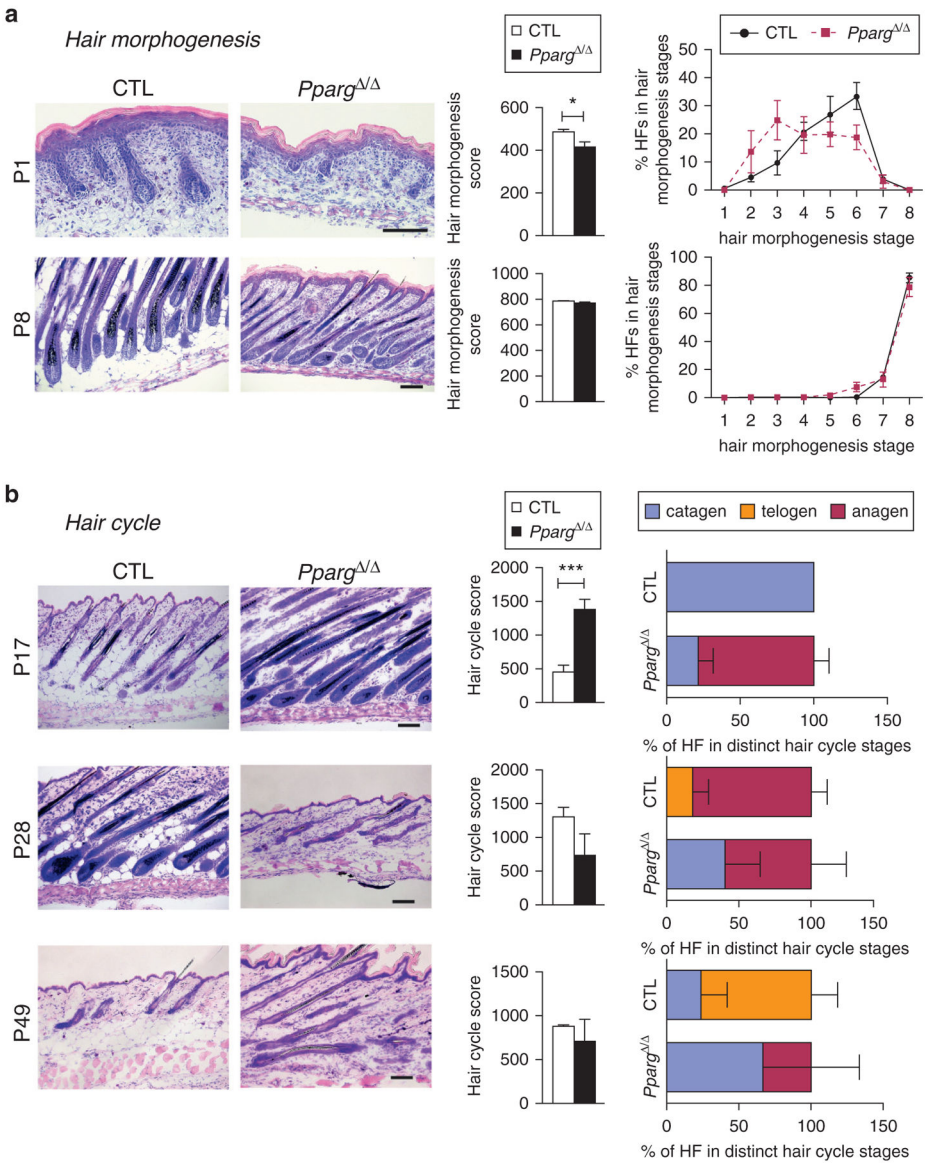

Figure 2. Delayed hair follicle morphogenesis and abnormal hair follicle cycling in *Pparg*$^{\Delta/\Delta}$ mice.

Quantitative histomorphometry of Giemsa-stained back skin cryosections from *Sox2-Cre*$^{tg/+}$*Pparg*$^{\Delta}$/*em*$^{\Delta}$ (*Pparg*$^{\Delta/\Delta}$) and control (CTL) mice collected at the indicated postnatal days. (**a**) Hair morphogenesis analysis at P1 and P8: representative pictures (left panel, scale bar = 100 μm), hair morphogenesis score (central panel), and percentage of HFs found in the different hair morphogenesis stages (right panel, n = 6). (**b**) Hair cycle progression analysis at P17 (catagen), P28 (anagen), and P49 (anagen): representative pictures (left panel, scale bar = 100 μm); hair cycle score (central panel); percentage of HFs found in the different hair cycle stage (right panel; n = 4–5). Score values are expressed as mean ± standard error of the mean. **P* < 0.05 and ****P* < 0.001, respectively. CTL, control; HF, hair follicle; P, postnatal day.

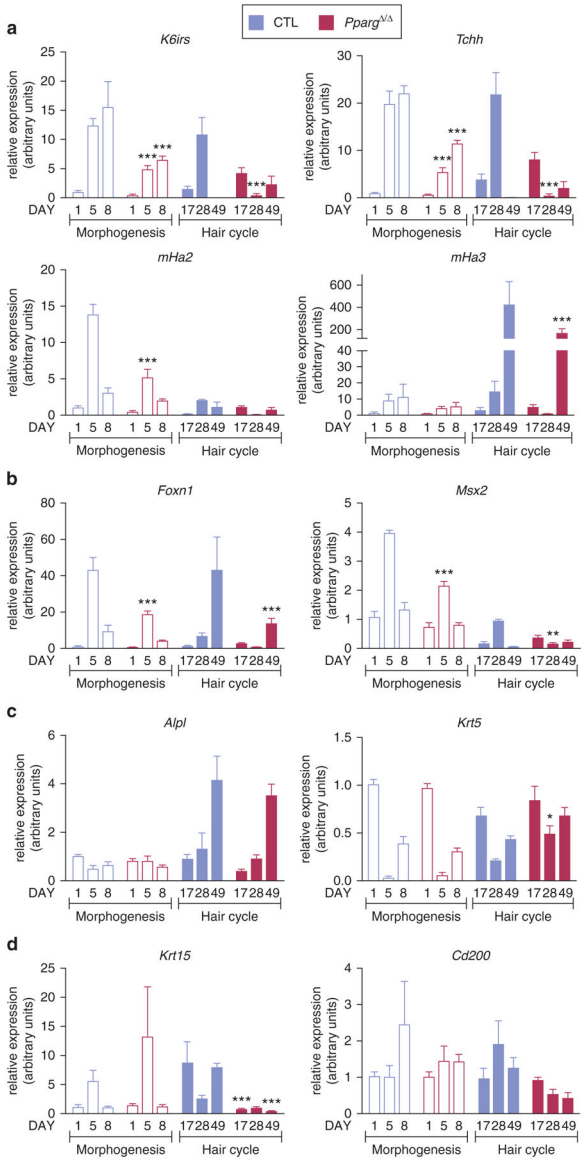

Figure 3. Molecular markers of the hair follicle cell populations are dysregulated in *Pparg*$^{\Delta/\Delta}$ mice during hair morphogenesis and cycling.

Quantitative PCR analysis of gene expression in skin from *Sox2-Cre*$^{tg/+}$ *Pparg*$^{\Delta}$*/em*$^{\Delta}$ (*Pparg*$^{\Delta/\Delta}$) (red bars) and control (CTL) (blue bars) mice. Hair morphogenesis (empty bars): P1 (n = 5), P5 (n = 6), and P8 (n = 5); hair cycle (filled bars): P17, P28, and P49 (n = 4). (**a**) *K6irs, Tchh,* and *mHa2* and *mHa3*. (**b**) *Foxn1* and *Msx2*. (**c**) *Alpl* and *Krt5*. (**d**) *Krt15* and *Cd200*. Data are normalized to *Eef1α1* and expressed as mean ± standard error of the mean. **P* < 0.05, ***P* < 0.01, and ****P* < 0.001, with respect to control expression at the same time point. CTL, control; P, postnatal day.

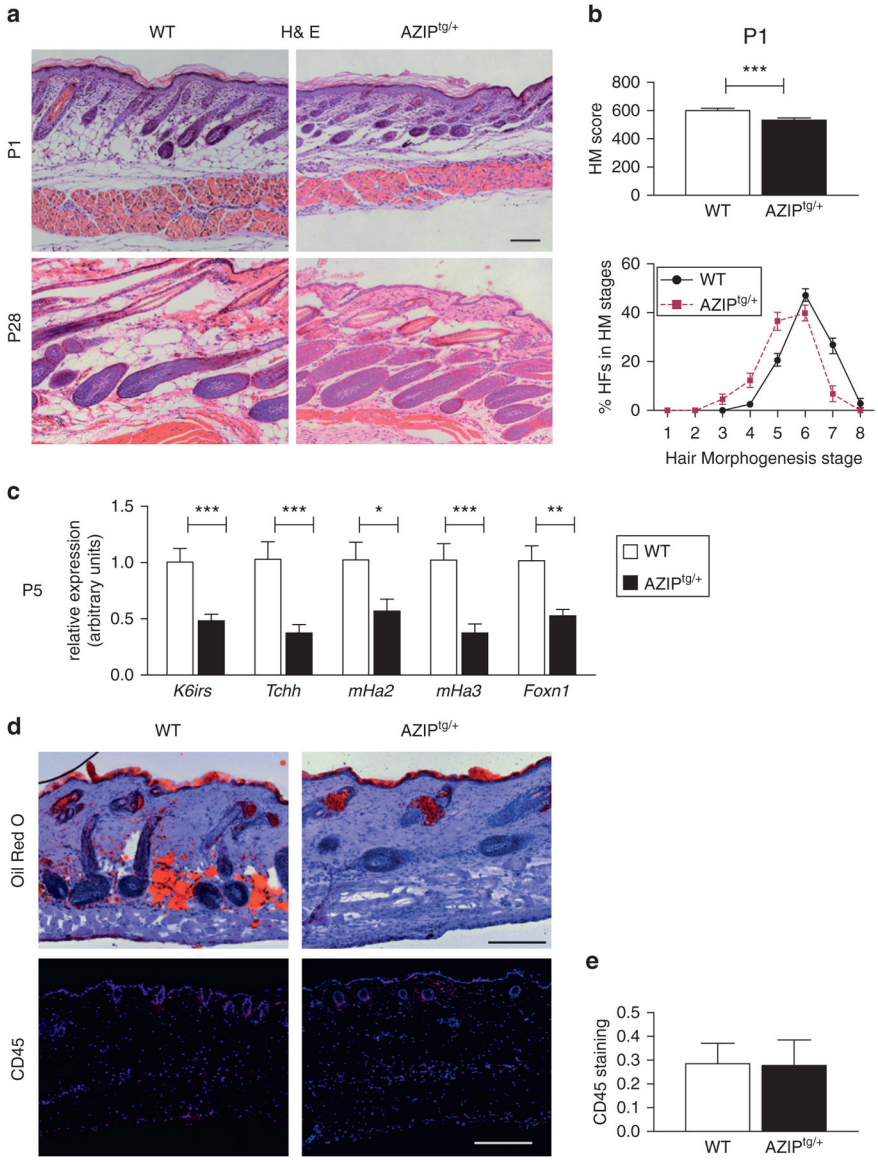

Figure 4. Delayed hair follicle morphogenesis in AZIP$^{tg/+}$ lipodystrophic mice.

Analysis of back skin sections from AZIP$^{tg/+}$ and WT mice. (**a**) Hematoxylin and eosin staining. Scale bar = 100 μm. (**b**) Quantitative histomorphometry at P1. Hair morphogenesis score (left). Percentage of HFs found in the different hair morphogenesis stages (right panel; n = 9–12). (**c**) Gene expression of *K6irs, Tchh, mHa2* and *mHa3,* and *Foxn1* in skin from AZIP$^{tg/+}$ and WT mice (P5). Data are normalized to *Eef1α1* and expressed as mean ± standard error of the mean (n = 7). (**d**) Oil Red O staining and CD45 immunostaining (leucocytes, in red) and (**e**) CD45 quantification. Scale bar = 200 μm. *$P < 0.05$, **$P < 0.01$ and ***$P < 0.001$, with respect to control at the same time point. H&E, hematoxylin and eosin; HM, hair morphogenesis; P, postnatal day; WT, wild type.

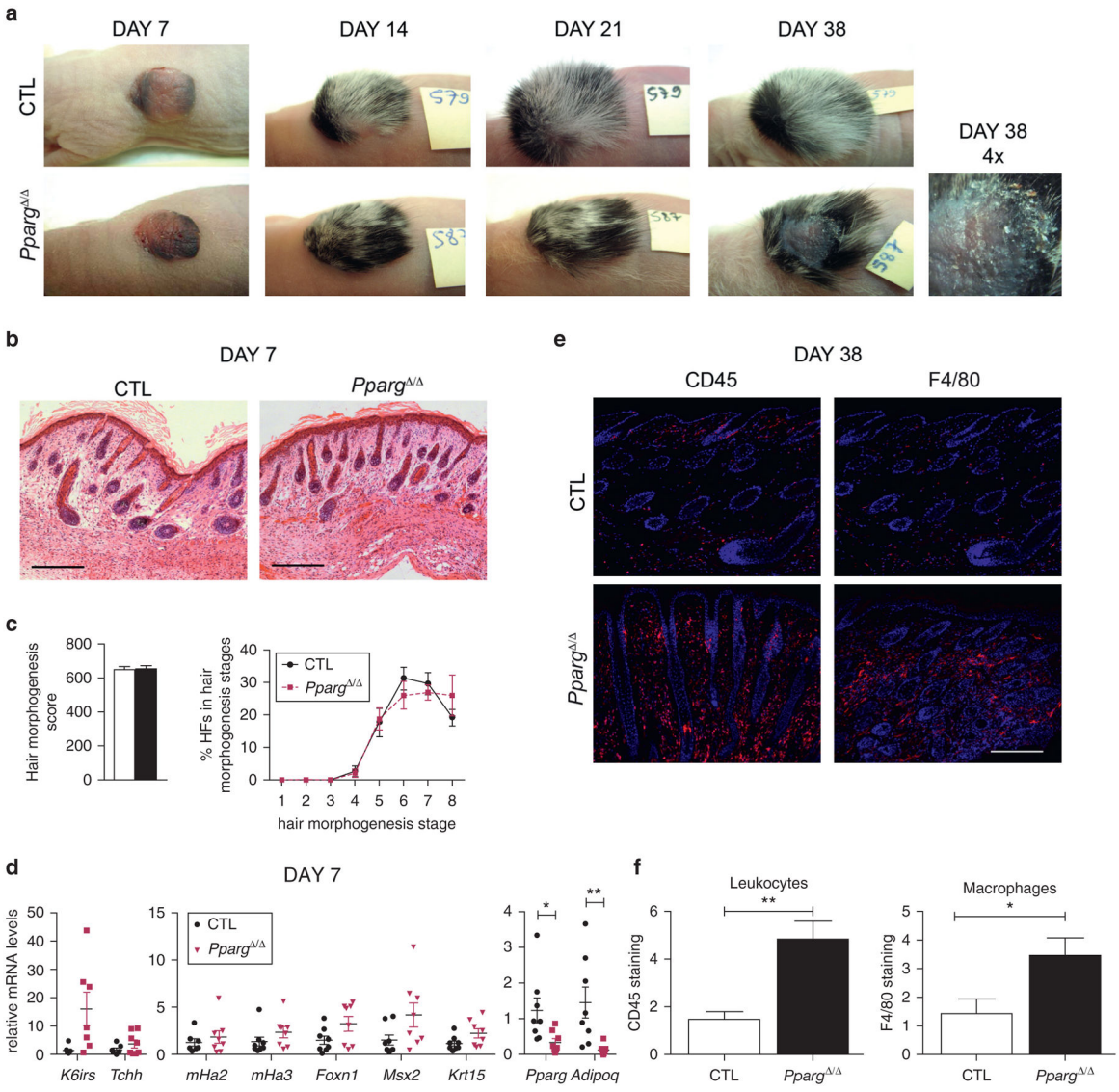

Figure 5. Skin graft experiments rescue *Pparg*$^{\Delta/\Delta}$ delayed hair morphogenesis but not late skin inflammation.

(**a**) Representative images of skin grafts from *Sox2-Cre*$^{tg/+}$ *Pparg*$^{\Delta em/\Delta}$ (*Pparg*$^{\Delta/\Delta}$) and control (CTL) embryos on *Foxn1*$^{nu/nu}$ mice. (**b**) Quantitative histomorphometry 7 days after engraftment. (**c**) Hair morphogenesis score (left); percentage of HFs in the different hair morphogenesis stages (right; n = 10–11). (**d**) Gene expression at day 7 of *K6irs*, *Tchh*, *mHa2* and *mHa3*, *Foxn1*, *Msx2*, *Krt15*, *Pparg*, and *Adipoq*. Data are normalized to *Eef1α1* and expressed as mean ± standard error of the mean (n = 8). (**e**) CD45 (leucocytes) and F4/80 (macrophages) immunostaining (red) at day 38 and (**f**) their quantification. Scale bar = 200 μm.*$P < 0.05$ and **$P < 0.01$. CTL, control; HF, hair follicle.

Table 1.

qPCR gene expression analysis of differentially regulated genes in the skin of *Pparg*$^{\Delta/\Delta}$ and AZIP$^{tg/+}$ mice

		Fold Change, *Pparg*$^{\Delta/\Delta}$ vs. CTL[1]		Fold Change, AZIP$^{tg/+}$vs. WT[2]
Pathway	**Gene**	**E17.5**	**P1**	**E17.5**
PPAR targets/adipose tissue function	*Adipoq*	−491	−204	−14.3
	Plin1	−36.3	−10.5	−13.1
	Fabp4	−2.4	−9.8	−2.9
	Rbp4	−3.2	−1.6	−2.6
Hair follicle	*Tshr*	−36.4	−57.3	−22.3
	Bmper	−4.7	−3.4	−2.3
Other functions	*Mgst1*	−2.0	−2.8	−2.13
	Cldn15	−3.8	−4.0	−2.1
	Enpep	−9.0	−1.6	−4.1

Abbreviations: CTL, control; E, embryonic day; P, postnatal day; WT, wild type.

[1] Gene expression evaluated by quantitative real-time PCR in the skin of *Pparg*$^{\Delta/\Delta}$ and control mice at E17.5 (n = 4) and P1 (n = 7).

[2] Gene expression evaluated by quantitative real-time PCR in the skin from AZIP$^{tg/+}$ and the respective control mice at E17.5 (n = 6).

J Invest Dermatol. Author manuscript; available in PMC 2021 May 10.